

# Lawrence Berkeley National Laboratory

## LBL Publications

### Title

Effect of Heteroatom and Doping on the Thermoelectric Properties of Poly(3-alkylchalcogenophenes)

### Permalink

<https://escholarship.org/uc/item/4fr7p53w>

### Journal

Advanced Energy Materials, 8(34)

### ISSN

1614-6832

### Authors

Gregory, Shawn A  
Menon, Akanksha K  
Ye, Shuyang  
[et al.](#)

### Publication Date

2018-12-01

### DOI

10.1002/aenm.201802419

Peer reviewed

# Effect of Heteroatom and Doping on the Thermoelectric Properties of Poly(3-alkylchalcogenophenes)

Shawn A. Gregory, Akanksha K. Menon, Shuyang Ye, Dwight S. Seferos, John R. Reynolds, and Shannon K. Yee\*

This study reports on the thermoelectric properties of poly(3-alkylchalcogenophene) thin films (500 nm) as a function of heteroatom (sulfur, selenium, tellurium), and how these properties change with dopant (ferric chloride) concentration. UV–vis–NIR spectroscopy shows that polaronic charge carriers are formed upon doping. Poly(3-alkyltellurophene) (P3RTe) is most easily doped followed by poly(3-alkylselenophene) (P3RSe) and poly(3-alkylthiophene) (P3RT), where R = 3,7-dimethyloctyl chain is the pendant alkyl group. Thermoelectric properties vary as functions of the heteroatom and doping level. At low dopant concentrations ( $\approx 1 \times 10^{-3}$  M), P3RTe shows the highest power factor of  $10 \mu\text{W m}^{-1} \text{K}^{-2}$ , while, at higher dopant concentrations ( $\approx 5 \times 10^{-3}$  M), P3RSe shows the highest power factor of  $13 \mu\text{W m}^{-1} \text{K}^{-2}$ . Most notably, it is found that the measured properties are consistent with Mott's polaron hopping model and not consistent with other transport models. Additionally, temperature-dependent conductivity measurements show that for a given dopant concentration, the activation energies for electronic transport decrease as the heteroatom is changed from sulfur to selenium to tellurium. Overall, this work presents a systematic study of poly(chalcogenophenes) and indicates the potential of polymers beyond P3HT by tuning the heteroatom and doping level for optimized thermoelectric performance.

## 1. Introduction

Polymer thermoelectric (TE) materials have garnered interest for energy harvesting applications because they are lightweight, flexible, and have an inherently low thermal conductivity.<sup>[1]</sup> Despite these advantages, many intrinsic semi-conducting polymers are not electrically conducting enough for thermoelectric applications. Doping can increase the electrical conductivity, but often results in a decrease in the Seebeck coefficient. For example, the electrical conductivity ( $\sigma$ ) of poly(3-hexylthiophene) (i.e., P3HT), which has been extensively studied,<sup>[2]</sup> ranges from  $10^{-5}$  to  $\approx 100 \text{ S cm}^{-1}$  while the Seebeck coefficient or thermopower ( $S$ ) ranges from 400 to  $25 \mu\text{V K}^{-1}$  with increased doping.<sup>[1a,3]</sup> This competing trend highlights the fundamental challenge in optimizing the power factor ( $S^2\sigma$ ) of TE materials, where tradeoffs between  $S$  and  $\sigma$  are conceded. In addition to doping, electronic properties can also be tuned by

tailoring the polymer chain length and substituents.<sup>[1a,b]</sup> For example, the electrical conductivity of doped poly(thieno)thiophene increases by three orders of magnitude as the molecular weight increases from 1 to 25 kDa.<sup>[4]</sup> Similarly, electrical conductivity can be increased through control of the heteroatoms present along the polymer backbone.<sup>[5]</sup>

These mechanisms for optimizing thermoelectric properties motivate the present investigation. Herein, we report the effects of varying the heteroatom from S, to Se, to Te in a class of poly(3-alkylchalcogenophenes), where the pendant alkyl group is a 3,7-dimethyloctyl chain,<sup>[6]</sup> and the effects of varying ferric chloride ( $\text{FeCl}_3$ ) dopant concentration on the overall thermoelectric properties. We also find that the measured thermoelectric properties are consistent with Mott's polaron hopping transport model around room temperature.

## 2. Background

A variety of oxidizing agents have been used to *p*-dope P3HT, including  $\text{FeCl}_3$ ,  $\text{F}_4\text{TCNQ}$ ,  $\text{I}_2$ ,  $\text{FeTos}$ , and  $\text{NOPF}_6$ .<sup>[1b,7]</sup> Oxidative doping induces morphological changes in the polymer that is a function of the doping procedure and the nature of dopant.<sup>[8]</sup>


S. A. Gregory  
School of Materials Science and Engineering  
Georgia Institute of Technology  
Atlanta, 30332 GA, USA

Dr. A. K. Menon, Prof. S. K. Yee  
G. W. Woodruff School of Mechanical Engineering  
Georgia Institute of Technology  
Atlanta, 30332 GA, USA  
E-mail: shannon.yee@me.gatech.edu

S. Ye, Prof. D. S. Seferos  
Department of Chemistry  
University of Toronto  
80 St. George Street, Toronto, Ontario M5S 1A1, Canada

Prof. D. S. Seferos  
Department of Chemical Engineering and Applied Chemistry  
University of Toronto  
200 College Street, Toronto, Ontario M5S 1A1, Canada

Prof. J. R. Reynolds  
School of Chemistry and Biochemistry  
School of Materials Science and Engineering  
Georgia Institute of Technology  
Atlanta, 30332 GA, USA

 The ORCID identification number(s) for the author(s) of this article can be found under <https://doi.org/10.1002/aenm.201802419>.

DOI: 10.1002/aenm.201802419

**Table 1.** Electrical conductivity and Seebeck coefficient as a function of temperature for various charge transport models for disordered materials.

Model	Electrical conductivity	Seebeck coefficient
Nearest neighbor hopping <sup>[14]</sup>	$\sigma = \sigma_1 \exp(-E_{A,1}/k_B T)$	$S = \left(\frac{k_B}{e}\right) \left(\frac{E_{A,1}}{k_B T} + A\right)$
Variable range hopping <sup>[15]</sup>	$\sigma = \sigma_2 \exp(-T_{0,2}/T)^{\frac{1}{d+1}}$	$S = S_{0,2}(T_{0,2} T)^{1/2}$
Mott mobility edge <sup>[17]</sup>	$\sigma = \sigma_3 \exp(-E_{A,3}/k_B T)$	$S = \left(\frac{k_B}{e}\right) \left(\frac{E_f - E_v}{k_B T} + 1\right)$
E-S variable range hopping <sup>[16]</sup>	$\sigma = \sigma_4 \exp(-T_{0,4}/T)^{\frac{1}{2}}$	$S = \text{constant}$
Mott polaron hopping <sup>[17]</sup>	$\sigma = \sigma_5 \exp(-(W_H + E_{A,5})/k_B T)$	$S = \left(\frac{k_B}{e}\right) \left(\frac{E_{A,5}}{k_B T} + C\right)$
Kang-Snyder transport model <sup>[10,18]</sup>	$\sigma = \int \sigma_{E_c}(T) \cdot ((E - E_t)/k_B T)^d \left(-\frac{df}{dE}\right) dE$	$S = \left(\frac{k_B}{e}\right) \int \sigma_{E_c}(E, T) \cdot ((E - E_t)/k_B T) \left(-\frac{df}{dE}\right) dE$

For example, Hong et al. showed that P3HT could be solution doped with FeCl<sub>3</sub> and then drop cast into a film with a lower power factor than P3HT that was wire bar-coated and then sequentially doped. The difference was attributed to the degree of crystallinity in the doped films, with aggregation occurring in solution doped films.<sup>[3b,9]</sup> Additionally, in their study it was found that thicker films have higher power factors than thinner films because dopants are more easily removed in the thinner films during the rinse step of the experimental procedure.<sup>[9]</sup>

Furthermore, oxidative doping electronically modifies conjugated polymers by abstracting electrons and forming polaronic charge carriers. These polarons are coulombically coupled with the oxidant anion, distort the local polymer structure, and create electronic states in the once forbidden bandgap.<sup>[1a,2a]</sup> At low doping concentrations, polaronic charge carriers are less mobile because they are trapped in the coulombic potential well created by dopant counterions. At higher dopant concentrations, the coulombic wells begin to overlap, thereby decreasing the energy barrier for polaronic transport and exhibiting a band-like electronic structure.<sup>[1a,10]</sup> Polaronic species can be probed by UV-vis spectroscopy, and the intensity of the optical transitions may be used as a qualitative and semiquantitative measure of doping.<sup>[3,11]</sup>

In addition to transporting charge that manifests as the electrical conductivity, mobile polaronic species also transport entropy under a thermal gradient, and this entropy transport manifests as the thermopower.<sup>[12]</sup> However,  $\sigma$  and  $S$  are inversely correlated and this coupling has made it challenging to develop thermoelectric materials with high power factors ( $S^2\sigma$ ). Furthermore, charge transport in doped polymers is fundamentally different than transport in metal or semiconducting crystalline materials because conducting polymers consist of spatially and energetically inhomogeneous domains.<sup>[1a,d,i,13]</sup> Inhomogeneous domains necessitate charge carriers to hop from one domain to another where the energy levels can be slightly different. Hence the Drude-Sommerfeld model ( $\sigma = ne\mu$ , where carriers are free particles in a spatially uniform electronic potential) is an inaccurate description of transport in doped polymeric systems, where thermoelectric discussions around mobility, scattering time, and Fermi level break down. For such disordered systems, there exists a myriad of transport models, including

nearest-neighbor hopping (NNH),<sup>[14]</sup> variable range hopping (VRH),<sup>[15]</sup> Efros-Shklovskii hopping (ESH),<sup>[16]</sup> Mott Polaron hopping,<sup>[17]</sup> and the mobility edge (ME) models.<sup>[17]</sup> Additionally, Kang and Snyder recently introduced an empirical charge transport model specifically for conducting polymers,<sup>[10,18]</sup> which in a general manner, results in pre-factors and exponents that capture trends in literature but do not provide a physical description. A summary of these transport models for disordered systems and their temperature dependence is shown in **Table 1**.

To our knowledge, there has not been a systematic study correlating the identity of the heteroatom in polyheterocycles with i) the doping process, ii) the resulting thermoelectric properties, and iii) the charge transport mechanism. Herein, we examine how the extent of ferric chloride doping impacts the thermoelectric properties of the regioregular forms of poly(3-alkylthiophene) (P3RT), poly(3-alkylselenophene) (P3RSe) and poly(3-alkyltellurophene) (P3RTe), where  $R$  is the alkyl solvating group 3,7-dimethyloctyl, as shown in **Figure 1**. Using UV-vis, we find that polaronic carriers are formed upon doping that leads to an increase in light absorption at low energies. Comparing between the three polymers, film dip-doping for 3 min in a fixed dopant concentration of  $1 \times 10^{-3}$  M, the electrical conductivity increases as we change the heteroatom from S to Se to Te, while the thermopower follows the opposite trend. At higher doping concentrations of  $20 \times 10^{-3}$  M, we find that the thermopower of all three polymers approaches  $\approx 30 \mu\text{V K}^{-1}$ , with P3RTe and P3RSe appearing to be over doped. Finally, by measuring thermoelectric properties as a function of temperature, we conclude that charge transport in these doped poly(3-alkylchalcogenophenes) near room temperature, is best described by thermally activated polaron hopping (i.e., Mott polaron hopping).<sup>[17]</sup> These optical and electrical measurements show that the heteroatom strongly influences the doping susceptibility, and that the thermoelectric properties can be tuned systematically.

### 3. Results and Discussion

High molecular weight (43 – 49.8 kDa), narrow dispersity ( $\mathcal{D} < 1.2$ ), and regioregular P3RT, P3RSe, and P3RTe were used

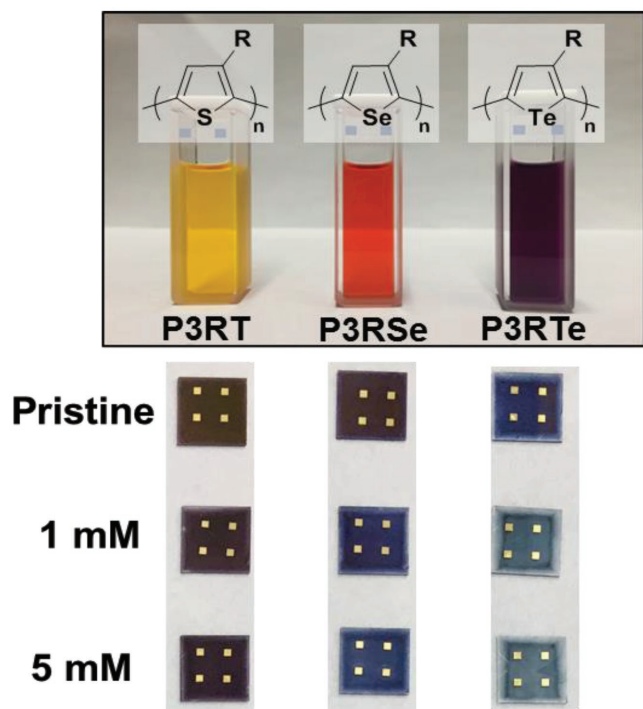


**Figure 1.** Poly(3-alkylchalcogenophenes) under study with R = 3,7-dimethyloctyl side chains. Cuvettes show pristine chalcogenophenes solvated in chloroform. Films were prepared by blade coating 30 mg mL<sup>-1</sup> solutions from chlorobenzene and then dip-doped in acetonitrile solutions of FeCl<sub>3</sub>. Films become increasingly visibly transparent as dopant concentration increases.

for this study. Films of P3RT, P3RSe, and P3RTe were prepared by blade coating from chlorobenzene solutions and were subsequently dip-doped for 3 min in ferric chloride solutions of varying molarities. After doping, the films were rinsed in acetonitrile, air dried, and then measured or characterized under ambient conditions. Detailed procedures for sample preparation and characterization are provided in the Experimental Section and Table S2, Figures S1 and S2 (Supporting Information).

### 3.1. Optical Absorption Spectra Show Doping-Induced Polaronic States

UV-vis spectroscopy was used to provide insight into the extent of charge transfer between the poly(3-alkylchalcogenophenes) upon doping with ferric chloride. **Figure 2** shows the absorbance spectra for P3RT, P3RSe, and P3RTe films at different doping concentrations; insets show the emerging (bi)polaronic transition as pristine polymers are doped with  $5 \times 10^{-3}$  M FeCl<sub>3</sub> solutions. In the pristine polymers, we observe a bathochromic (red) shift of the  $\pi-\pi^*$  absorbance peaks as the heteroatom is changed from S to Se to Te. The bathochromic shift is likely because the heteroatom atomic bandgap (electronegativity) decreases from S to Se to Te, and when linearly combined with other conjugated carbon molecular orbitals, the polymer FMOs are energetically close, thereby leading to a smaller optical bandgap. Upon doping with FeCl<sub>3</sub>, polaronic species are created, as seen by the emergence of an absorbance peak in the

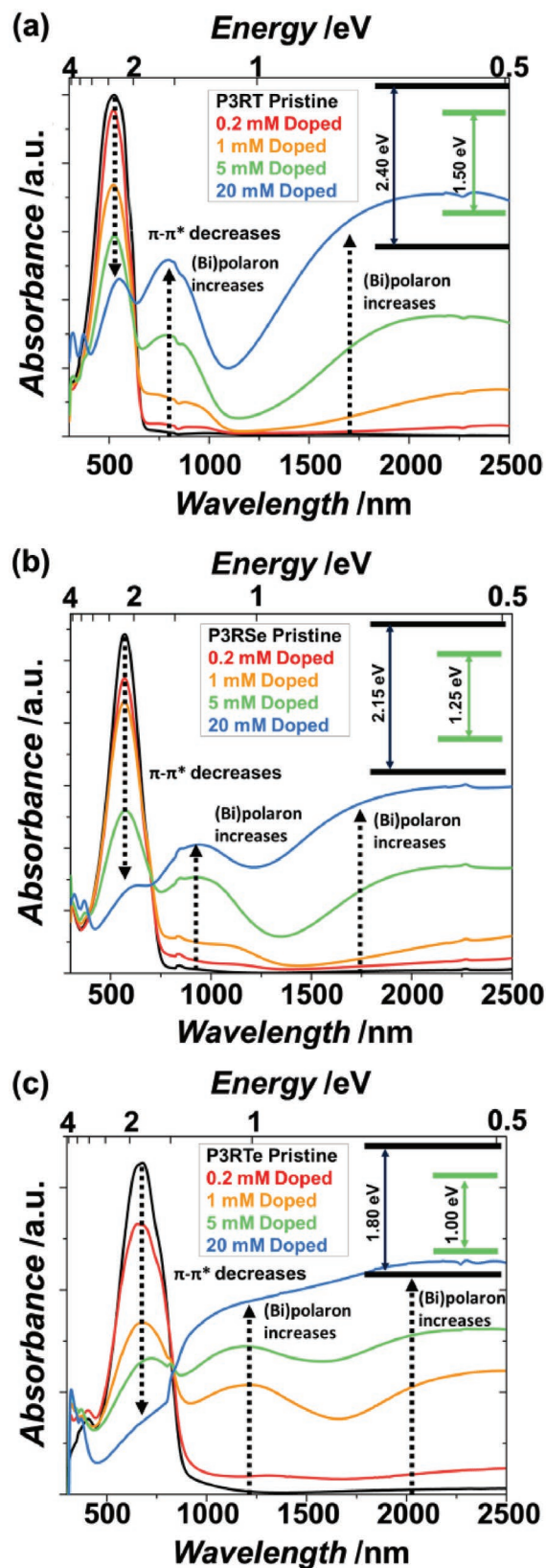


**Figure 2.** UV-vis spectra for poly(3-alkylchalcogenophene) films at varying dopant concentrations: a) P3RT, b) P3RSe, c) P3RTe. Insets show the change in the optical bandgap as each polymer is doped to  $5 \times 10^{-3}$  M.

NIR (see Table S3, Supporting Information). Worth noting is that the solvating group on these poly(3-alkylchalcogenophenes) is a 3,7-dimethyloctyl chain, and not the canonical hexyl group (utilized to enhance overall solubility), yet the P3RT  $\pi$ - $\pi^*$  and polaronic absorbance peaks in this study are well aligned with previous reports for other polythiophenes.<sup>[5b,11b,19]</sup>

The extent of doping manifests as a decrease of the  $\pi$ - $\pi^*$  absorbance intensity, which becomes more prominent as the heteroatom is changed from S to Se to Te. The extent of doping also manifests in the emergence of the polaron and (bi) polaron absorbance peaks. Longer wavelength (bi) polaronic peaks emerge at lower dopant concentrations as the heteroatom is changed from S to Se to Te. Although doping extent is a nontrivial convolution of material, kinetic, and thermodynamic variables, we attribute P3RTe's relatively high susceptibility to FeCl<sub>3</sub> doping to its smaller band gap (higher electron polarizability) despite showing a HOMO level slightly more stable (0.1–0.2 eV) than P3RSe and P3RT (Figure S3, Supporting Information).<sup>[20]</sup> CV data agree with the UV-vis data in Figure 2 and shows that P3RTe oxidizes at lower potentials compared to P3RSe and P3RT (Figure S4, Supporting Information). Last, (bi) polaron peaks in the MIR broaden as the heteroatom is varied from S ( $z = 16$ ) to Se ( $z = 32$ ) to Te ( $z = 54$ ), and we hypothesize this is because Te introduces additional electrons, electronic states, and effective atomic shielding of valence electrons in comparison to Se and S, which permits more band-like distribution of electronic states.

### 3.2. Heavier Heteroatoms Result in Large Electrical Conductivities at Low Doping Concentrations and are Overdoped at High Doping Concentrations

To understand how the dopant-induced electronic states impact thermoelectric properties, electrical conductivity, and thermopower for doped poly(3-alkylchalcogenophene) films were measured at four different dopant concentrations at room temperature, as depicted in Figure 3. It has been shown that the electrical conductivity is (exponentially) sensitive to small changes in dopant concentration at very low and at very high dopant concentrations.<sup>[11b]</sup> Dopants initially increase electrical conductivity by homogenizing the electronic landscape, but excess dopants decrease conductivity by creating scattering sites, microstructural changes, and/or bipolarons.<sup>[11b,21]</sup> We found that sequential doping for 3 min in  $1 \times 10^{-3}$  and  $5 \times 10^{-3}$  M solutions yielded more repeatable results than doping in  $0.2 \times 10^{-3}$  and  $20 \times 10^{-3}$  M solutions; we further attribute this repeatability to the conductivity being exponentially sensitive at low ( $<0.2 \times 10^{-3}$  M) and high doping ( $>20 \times 10^{-3}$  M) levels.<sup>[11b]</sup> The repeatability of the  $1 \times 10^{-3}$  and  $5 \times 10^{-3}$  M doped films is shown with error bars in Figure 3 that represent the sample-to-sample variation.

At a low doping level of  $0.2 \times 10^{-3}$  M, P3RTe is the only polymer that shows appreciable electrical conductivity, with a value that is 100× larger than P3RT at the same dopant concentration. At  $1 \times 10^{-3}$  M dopant concentration, P3RTe still exhibits the highest electrical conductivity and the lowest thermopower ( $46 \text{ S cm}^{-1}$ ,  $51 \mu\text{V K}^{-1}$ ), followed by P3HSe ( $29 \text{ S cm}^{-1}$ ,  $89 \mu\text{V K}^{-1}$ ), and last P3RT shows the lowest electrical conductivity and

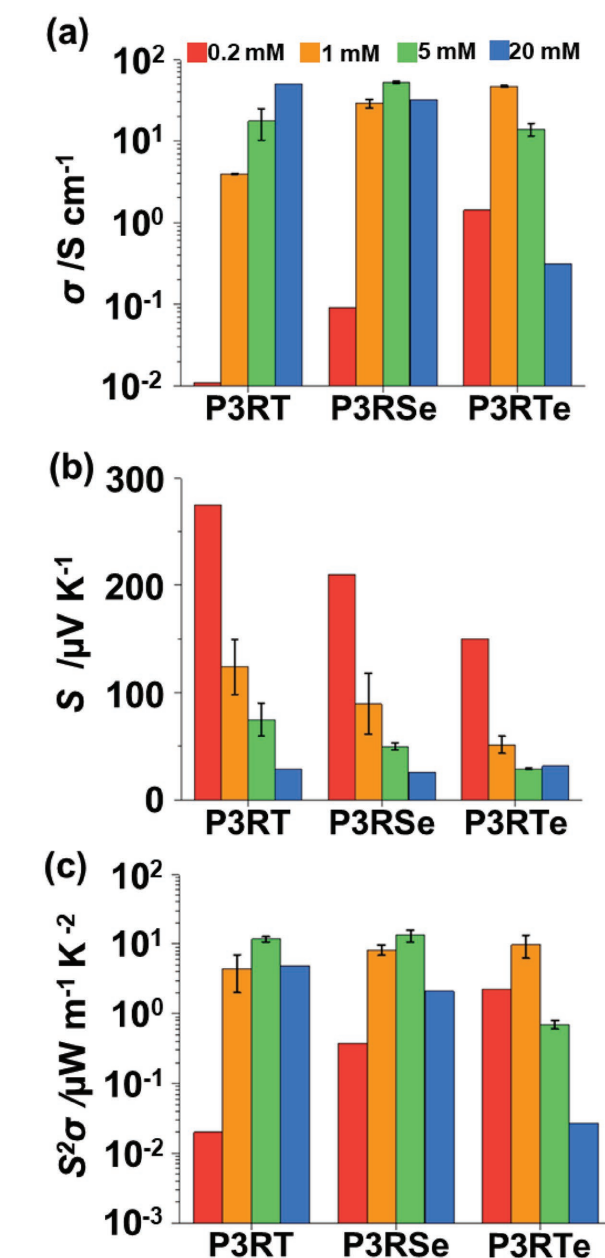


**Figure 3.** Thermoelectric properties for poly(3-alkylchalcogenophene) films doped with four different FeCl<sub>3</sub> solutions of  $0.2 \times 10^{-3}$ ,  $1 \times 10^{-3}$ ,  $5 \times 10^{-3}$ , and  $20 \times 10^{-3}$  M: a) Electrical conductivity. b) Thermopower. c) Power factor. Error bars capture sample-to-sample variations.

highest thermopower ( $4 \text{ S cm}^{-1}$ ,  $124 \mu\text{V K}^{-1}$ ). The positive thermopower values confirm that these polymers are all hole-transporting materials (p-type semiconductors). From S to Se to Te, the electrical conductivity increases; this aligns with the doping susceptibility data shown in the CV and UV-vis (Figure S4, Supporting Information and Figure 2, respectively). In contrast, the thermopower decreases from S to Se to Te, likely because the dopant-induced electronic states decrease the asymmetry of electronic states about the chemical potential, as seen by the smaller optical band gap (and likely transport gap) in

Figure 2.<sup>[11a,22]</sup> This trade-off between  $S$  and  $\sigma$  with increasing carrier concentration is consistent with literature reports on P3HT and other semiconducting polymers.<sup>[10,23]</sup>

At a higher dopant concentration of  $5 \times 10^{-3}$  M, P3RT and P3RSe both show a higher electrical conductivity and a lower thermopower ( $17 \text{ S cm}^{-1}$ ,  $75 \text{ } \mu\text{V K}^{-1}$  for P3RT and  $52 \text{ S cm}^{-1}$ ,  $50 \text{ } \mu\text{V K}^{-1}$  for P3RSe) when compared to the  $1 \times 10^{-3}$  M doping. This is attributed to a higher dopant concentration enabling a higher level of doping in the film and the formation of more polaronic carriers. P3RTe also shows a lower thermopower at  $5 \times 10^{-3}$  M, but this is accompanied by a decrease in the electrical conductivity ( $14 \text{ S cm}^{-1}$ ,  $29 \text{ } \mu\text{V K}^{-1}$ ). We attribute the decrease in electrical conductivity to the P3RTe becoming overdoped. Although more charge carriers are formed as evidenced in the UV-vis polaronic peaks (see Figure 2c), we hypothesize that the  $5 \times 10^{-3}$  M doping results in carrier scattering (i.e., decrease in carrier mobility) by either i) preferentially forming (bi) polarons that scatter more than polarons,<sup>[11b]</sup> or ii) oversaturating the polymer with dopant species, thereby creating traps in the morphological and/or electronic landscape.<sup>[24]</sup>

Upon further increasing the doping concentration to  $20 \times 10^{-3}$  M, both P3RSe and P3RTe films appear to become overdoped as evidenced by the simultaneous decrease in electrical conductivity and thermopower, while P3RT is not overdoped and attains the highest conductivity of  $50 \text{ S cm}^{-1}$ . We note that at this concentration, P3RTe displays a lower electrical conductivity when compared to the  $5 \times 10^{-3}$  M sample (which was also overdoped), but the thermopower remains relatively unchanged (within measurement error). We attribute this to the presence of excess charge carriers at similar energy that hinders charge transport and reduces conductivity but has little effect on thermopower. This is analogous to impurity scattering (which is an energy-independent scattering event in crystalline inorganic semiconductors) that reduces conductivity, but has no impact on the thermopower because it does not change the energy-dependent landscape.<sup>[25]</sup> We also observe that over-doped systems begin to deviate from the  $S \propto \sigma^{-1/4}$  empirical trend proposed by Glauddell et al. (Figure S7, Supporting Information).<sup>[10]</sup> Overdoped systems deviate from the  $S$ - $\sigma$  coupling because thermopower remains relatively constant while electrical conductivity exponentially decreases.

Last, power factors were calculated with P3RT and P3RSe reaching similar maximum values of  $12 \text{ } \mu\text{W m}^{-1} \text{ K}^{-2}$  and  $13 \text{ } \mu\text{W m}^{-1} \text{ K}^{-2}$ , respectively, at a doping concentration of  $5 \times 10^{-3}$  M, where P3RTe reached a maximum power factor of  $10 \text{ } \mu\text{W m}^{-1} \text{ K}^{-2}$  at a  $1 \times 10^{-3}$  M dopant concentration. It is expected that thermoelectric properties can be further improved by using vapor doping, which has been shown to have minimal consequences on film morphology in comparison to solution doping.<sup>[3b]</sup>

### 3.3. Heteroatom and Doping Impact Charge Transport that Proceeds via Thermally Activated Polaron Hopping

To understand how the heteroatom affects charge transport in these polymers near room temperature, we performed temperature-dependent thermoelectric measurements and related them to the transport models presented in Table 1. By

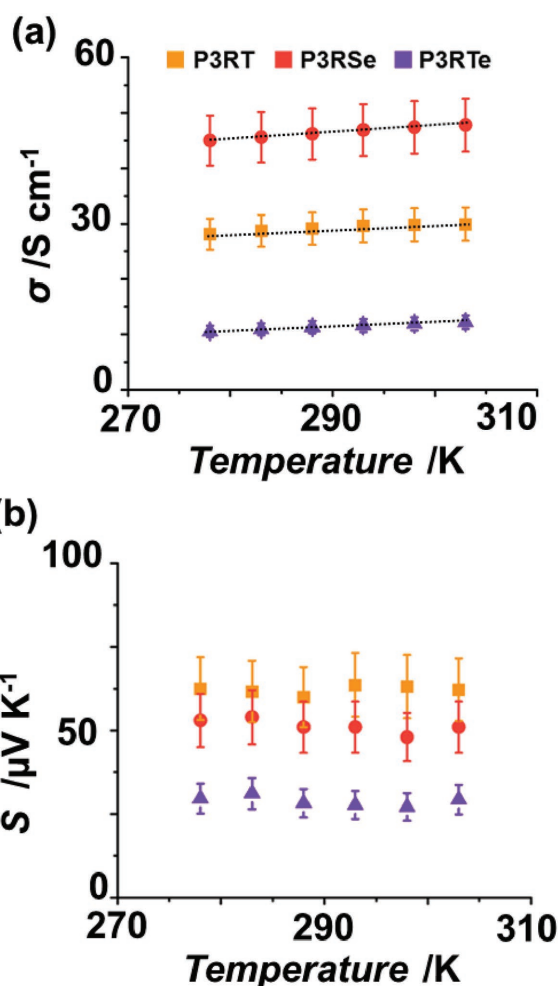
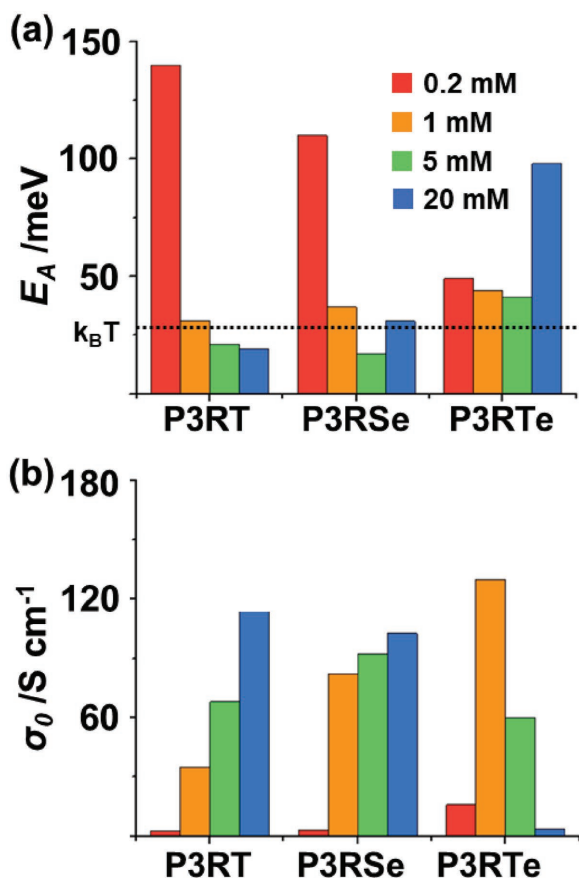


Figure 4. a) Electrical conductivity as a function of temperature for  $5 \times 10^{-3}$  M doped samples. b) Thermopower as a function of temperature for  $5 \times 10^{-3}$  M doped samples.

measuring both the electrical conductivity and the thermopower as functions of temperature, the transport mechanism can be elucidated. However, the heterogeneous nature (ordered domains connected by amorphous domains) of these poly(3-alkylchalcogenophenes) and other doped polymers<sup>[1j,10]</sup> complicates this analysis. Nevertheless, the underlying ideas of a pre-exponential factor,  $\sigma_0$  (which is independent of temperature but depends on morphology) and an activation energy,  $E_A$  (also referred to as the transport barrier) are common to all transport models. To extract these parameters for each poly(3-alkylchalcogenophene), electrical conductivity and thermopower measurements were performed at different dopant concentrations from 270 to 320 K; Figure 4 shows this for the  $5 \times 10^{-3}$  M doped polymers. This temperature range was selected to mitigate thermally induced de-doping, which was found to occur above 320 K (see Figure S5, Supporting Information), and is well documented in polythiophenes.<sup>[26]</sup>

We observe that the electrical conductivity for all poly(3-alkylchalcogenophenes) increases with temperature, indicating a thermally activated mechanism that is expected for semiconducting materials. In this range, thermopower measurements



**Figure 5.** a) Activation energy or transport barrier,  $E_A$ , extracted from electrical conductivity. b) Conductivity pre-factor,  $\sigma_0$ . Activation energies and the conductivity pre-factor are extracted from Mott's polaron hopping model using the dependence of electrical conductivity on temperature.

show a weak dependence on temperature, which is characteristic of hopping transport. These trends are suggestive of disorder but do not necessarily describe transport in the ordered domains of these heterogeneous systems. We also observe that  $S$  and  $\sigma$  show different activation energies indicating that thermally assisted polaronic hopping is a suitable transport framework for these polymers. In Mott's polaron hopping model, the electrical conductivity has an activation energy that comprises the donor ionization energy and polaron hopping activation energy, while the Seebeck coefficient is only related to the donor ionization energy normalized by  $k_B T$  plus a relatively large constant term.<sup>[17]</sup> Fritzsche equated this constant term with the density of electronic states, and Xuan et al. related this with the concentration of (bi)polaronic charge carriers; the thermopower values in Figure 4b and Figure S5 (Supporting Information) are consistent with their reports.<sup>[3a,22]</sup>

The transport activation energy,  $E_A$  and conductivity pre-factor,  $\sigma_0$  can be extracted from  $\sigma$  versus  $T$  plots for each poly(3-alkylchalcogenophene) at a given dopant concentration as shown in Figure 5. Prior work suggests that the transport barrier is proportional to the energy separating two (bi)polaronic sites located near the chemical potential.<sup>[3a,17,27]</sup> Figure 5a shows that as P3RT is increasingly doped, more polaronic states are created, resulting in a decrease in the activation energy. This

trend also holds true for P3RSe and P3RTe, until they become overdoped at  $20 \times 10^{-3}$  M and concomitantly show a nearly nonexistent  $\pi$ - $\pi^*$  absorbance peak and broad (bi)polaronic peaks (see Figure 2). We hypothesize that at these high doping levels excessive charge carriers impede electronic transfer, thus increasing the transport barrier.

Figure 5b shows the conductivity pre-factor as a function of doping for each poly(3-alkylchalcogenophene). This term is dependent on the number of electronic states and hopping probability, which are directly related to the charge carrier concentration and hopping distance, and morphology.<sup>[3a,17]</sup> For P3RT and P3RSe, the pre-factor term increases with increasing doping, with a large increase from  $0.2 \times 10^{-3}$  to  $1 \times 10^{-3}$  M doping. This is likely due to the i) smoothed energetic landscape, ii) increased available states and carriers, and iii) larger hopping distances enabled by the smooth landscape.

P3RTe is an interesting case study for charge transport. At low dopant concentrations ( $\leq 1 \times 10^{-3}$  M), P3RTe shows the lowest activation energy because it has a small bandgap and is easily doped, and we attribute P3RTe's large conductivity pre-factor to the relatively small interchain (seen in analogous pristine XRD measurements) and interplanar distances (seen in UV-vis doping extent and S1)<sup>[6,21]</sup> This may be because P3RTe is either unable to accommodate the large influx of dopant in its relatively small interlayer channels (which causes the film microstructure to swell),<sup>[5c,d,21]</sup> or because less mobile (bi) polarons are formed, as was hypothesized in the previous section. Although more carriers are created at  $5 \times 10^{-3}$  and  $20 \times 10^{-3}$  M as evidenced from the UV-vis, the contribution of these carriers to conductivity may be diminished by other factors, resulting in a morphology-limited conductivity.<sup>[10]</sup> The thermopower is found to approach  $\approx +30 \mu V\ K^{-1}$  for doping concentrations of  $\geq 5 \times 10^{-3}$  M, which further suggests that these additional carriers do not participate in transport and that film microstructural changes due to dopant introduction only impact electrical conductivity material constants. Our observation that the Seebeck coefficient is independent of film morphology and charge carrier (energy-independent) scattering is well aligned with prior organic thermoelectric studies.<sup>[23c,28]</sup>

## 4. Conclusions

In this work, we have shown that by systematically varying the heteroatom in poly(3-alkylchalcogenophenes), the thermoelectric properties can be tuned by doping with ferric chloride. Moving from S to Se to Te, the optical band gap shrinks, and the energy states move closer to the chemical potential. As a result, the thermopower decreases, while the electrical conductivity increases. Therefore, at low dopant concentrations, P3RTe and P3RSe can achieve power factors of over  $10 \mu W\ m^{-1}\ K^{-2}$ , which is comparable to highly doped polythiophenes. The charge transport mechanism in all three poly(3-alkylchalcogenophenes) follows Mott's polaron hopping transport and reflects the inherent disorder in these heterogeneous systems. The observations reported herein lay the groundwork for understanding thermoelectric transport through doping studies of this poly(3-alkylchalcogenophene) series, towards the goal of developing high-performance thermoelectric polymers.

## 5. Experimental Section

**Chalcogenophene Synthesis:** 3,7-dimethyloctyl side chains were installed at the 3-position following literature procedures.<sup>[29]</sup> The poly(3-alkylthiophene), poly(3-alkylselenophene), and poly(3-alkyltellurophene) polymers were synthesized by catalyst transfer polycondensation with similar catalyst loading followed by purification by Soxhlet extraction and column chromatography.

**Polymer Characterization:** All polymers were prepared with high and similar  $M_n$  (43–48.9 kDa) and narrow dispersity (about 1.2), which is confirmed by gel permeation chromatography (GPC) referring to polystyrene standards. Compared to the corresponding monomer, the signals in  $^1\text{H}$  NMR spectra are broadened, which is characteristic of high  $M_n$  polymer. Only one singlet (6.99, 7.11, and 7.40 ppm) was found in the aromatic region corresponding to the aromatic proton at the 3-position of the heterocycles. Additionally, the three polymers show a high regioregularity over 96% estimated by integration ratio of regioregular and regiorandom methylene protons.

**Film Fabrication and Characterization: Blade Coating**—All film preparation and doping procedures were performed in air. Films were prepared by blade-coating from 30 mg mL<sup>-1</sup> solutions of chalcogenophene in chlorobenzene (Zehntner Testing Instruments, ZAA 2300). Glass substrates (1 cm × 1 cm, 500 μm thick) were pretreated by sonication in DI water, acetone, and isopropanol prior to the blade coating process. Due to different viscosities of the polymer solutions, variable speeds and blade heights were used: 25 mm s<sup>-1</sup> and 650 μm for P3RT, 30 mm s<sup>-1</sup> and 670 μm for P3RSe, and 28 mm s<sup>-1</sup> and 670 μm for P3RTe. This was done to ensure that the final thickness of all films was ≈500 nm as measured via profilometry using a Bruker DektakXT profilometer. Four gold contact pads (1 mm × 1 mm, ≈100 nm thick) were then deposited on the prepared films using a shadow mask in an e-beam evaporator.

**Doping:** Dopant solutions at different concentrations were prepared by dissolving anhydrous ferric chloride in anhydrous acetonitrile to yield solution molarities of  $0.2 \times 10^{-3}$ ,  $1 \times 10^{-3}$ ,  $5 \times 10^{-3}$ , and  $20 \times 10^{-3}$  M. Films were dip-doped for 3 min. After doping, films were quickly rinsed in acetonitrile to remove excess FeCl<sub>3</sub> and were then placed on a covered hot plate for one minute to dry. Thermoelectric measurements were performed immediately, and multiple samples were prepared to capture sample-to-sample variations, generating representative error bars that are reported as the standard deviation.

**UV–Vis–NIR measurements:** A Varian Cary 5000 UV–Vis–NIR spectrophotometer was used to characterize absorption profiles of the chalcogenophene films from 300 to 2500 nm. Films for UV–vis–NIR analysis were doped, using the same doping procedure that was used before thermoelectric measurements, and then optically characterized.

**Thermoelectric Measurements:** Electrical conductivity and Seebeck measurements were made on a custom setup.<sup>[28]</sup> Micromanipulators with tungsten tips were used to make electrical contact to the gold contact pads and in-plane electrical conductivity was acquired using the four-probe Van der Pauw technique. The Seebeck coefficient was measured by suspending the sample between two temperature-controlled Peltier units (separated ≈3 mm) and applying a series of temperature differences up to  $\Delta T = 10$  K between the stages. The thermoelectric voltage was measured between two contact pads on separate stages using the probe tips, while the temperature of each pad was measured with a K-type thermocouple in close proximity to the probe tips. Voltage and temperature data were acquired using a Keithley 2700 DMM with a 7708 Mux card via a LabVIEW interface. The Seebeck coefficient was extracted as the slope of the  $V$  versus  $\Delta T$  plot. All measurements were made in ambient atmosphere and under illumination, as the thermoelectric properties remained stable and unaffected over the measurement time frame (Figure S6, Supporting Information).

## Supporting Information

Supporting Information is available from the Wiley Online Library or from the author.

## Acknowledgements

S.A.G. and A.K.M. contributed equally to this work. This work was supported by the Air Force Office of Scientific Research under Award FA9550-15-1-0145. A.K.M. acknowledges support from the Qatar Foundation's Qatar Research Leadership Program (QRLP). The authors acknowledge experimental apparatus support from the Center for Organic Photonics and Electronics (COPE) at Georgia Tech. D.S.S. and S.Y. acknowledge support from the NSERC of Canada. Last, the authors thank James Ponder and Rylan Wolfe for their insightful discussions.

## Conflict of Interest

The authors declare no conflict of interest.

## Keywords

charge transport, conducting polymers, doping, organic electronics, thermoelectrics

Received: August 4, 2018

Revised: August 30, 2018

Published online:

- [1] a) O. Bubnova, X. Crispin, *Energy Environ. Sci.* **2012**, *5*, 9345; b) R. Kroon, D. A. Mengistie, D. Kiefer, J. Hynynen, J. D. Ryan, L. Yu, C. Muller, *Chem. Soc. Rev.* **2016**, *45*, 6147; c) O. Bubnova, Z. U. Khan, A. Malti, S. Braun, M. Fahlman, M. Berggren, X. Crispin, *Nat. Mater.* **2011**, *10*, 429; d) O. Bubnova, Z. U. Khan, H. Wang, S. Braun, D. R. Evans, M. Fabretto, P. Hojati-Talemi, D. Dagnelund, J. B. Arlin, Y. H. Geerts, S. Desbief, D. W. Breiby, J. W. Andreasen, R. Lazzaroni, W. M. Chen, I. Zozoulenko, M. Fahlman, P. J. Murphy, M. Berggren, X. Crispin, *Nat. Mater.* **2014**, *13*, 190; e) A. K. Menon, E. Uzunlar, R. M. W. Wolfe, J. R. Reynolds, S. R. Marder, S. K. Yee, *J. Appl. Polym. Sci.* **2017**, *134*, 44402; f) A. K. Menon, S. K. Yee, *J. Appl. Phys.* **2016**, *119*, 055501 g) Q. Zhang, Y. Sun, W. Xu, D. Zhu, *Adv. Mater.* **2014**, *26*, 6829; h) M. Culebras, C. M. Gomez, A. Cantarero, *Materials* **2014**, *7*, 6701; i) N. Lu, L. Li, M. Liu, *Phys. Chem. Chem. Phys.* **2016**, *18*, 19503; j) B. Russ, A. Glaudell, J. J. Urban, M. L. Chabiny, R. A. Segalman, *Nat. Rev. Mater.* **2016**, *1*, 16050; k) A. K. Menon, R. M. W. Wolfe, S. R. Marder, J. R. Reynolds, S. K. Yee, *Adv. Funct. Mater.* **2018**, *28*, 1801620; l) R. M. W. Wolfe, A. K. Menon, T. R. Fletcher, S. R. Marder, J. R. Reynolds, S. K. Yee, *Adv. Funct. Mater.* **2018**, *28*, 1801620.
- [2] a) J. L. Reddinger, J. R. Reynolds, *Adv. Polym. Sci.* **1999**, *145*, 57; b) R. D. McCullough, *Adv. Mater.* **1998**, *10*, 93; c) J. Roncali, *Chem. Rev.* **1997**, *97*, 173; d) T. P. Kaloni, P. K. Giesbrecht, G. Schreckenbach, M. S. Freund, *Chem. Mater.* **2017**, *29*, 10248.
- [3] a) Y. Xuan, X. Liu, S. Desbief, P. Leclère, M. Fahlman, R. Lazzaroni, M. Berggren, J. Cornil, D. Emin, X. Crispin, *Phys. Rev. B* **2010**, *82*, 115454; b) E. Lim, K. A. Peterson, G. M. Su, M. L. Chabiny, *Chem. Mater.* **2018**, *30*, 998.
- [4] a) J. Hynynen, D. Kiefer, L. Yu, R. Kroon, R. Munir, A. Amassian, M. Kemerink, C. Muller, *Macromolecules* **2017**, *50*, 8140; b) A. Gasperini, K. Sivula, *Macromolecules* **2013**, *46*, 9349.
- [5] a) J. Hollinger, D. Gao, D. S. Seferos, *Isr. J. Chem.* **2014**, *54*, 440; b) M. Al-Hashimi, Y. Han, J. Smith, H. S. Bazzi, S. Y. A. Alqaradawi, S. E. Watkins, T. D. Anthopoulos, M. Heeney, *Chem. Sci.* **2016**, *7*, 1093; c) L. Li, J. Hollinger, A. A. Jahnke, S. Petrov, D. S. Seferos, *Chem. Sci.* **2011**, *2*, 2306; d) A. A. Jahnke, B. Djukic,



- T. M. McCormick, E. Buchaca Domingo, C. Hellmann, Y. Lee, D. S. Seferos, *J. Am. Chem. Soc.* **2013**, *135*, 951.
- [6] E. I. Carrera, D. S. Seferos, *Macromolecules* **2015**, *48*, 297.
- [7] a) E. P. Tomlinson, S. Mukherjee, B. W. Boudouris, *Org. Electron.* **2017**, *51*, 243; b) Q. Zhang, Y. Sun, W. Xu, D. Zhu, *Energy Environ. Sci.* **2012**, *5*, 9639; c) Z. Fan, P. Li, D. Du, J. Ouyang, *Adv. Energy Mater.* **2017**, *7*, 1602116.
- [8] a) L. F. Warren, J. A. Walker, D. P. Anderson, C. G. Rhodes, L. J. Buckley, *J. Electrochem. Soc.* **1989**, *136*, 2286; b) X. Ren, F. Yang, X. Gao, S. Cheng, X. Zhang, H. Dong, W. Hu, *Adv. Energy Mater.* **2018**, *8*, 1801003.
- [9] C. T. Hong, Y. Yoo, Y. H. Kang, J. Ryu, S. Y. Cho, K.-S. Jang, *RSC Adv.* **2015**, *5*, 11385.
- [10] A. M. Glaudell, J. E. Cochran, S. N. Patel, M. L. Chabiny, *Adv. Energy Mater.* **2015**, *5*, 1401072.
- [11] a) A. Kahn, *Mater. Horiz.* **2016**, *3*, 7; b) J. Yamamoto, Y. Furukawa, *J. Phys. Chem. B* **2015**, *119*, 4788.
- [12] M. Chabiny, *Nat. Mater.* **2014**, *13*, 119.
- [13] S. Ihnatsenka, X. Crispin, I. V. Zozoulenko, *Phys. Rev. B* **2015**, *92*, 035201.
- [14] M. Cutler, N. F. Mott, *Phys. Rev.* **1969**, *181*, 1336.
- [15] T. E. Whall, *J. Phys. C: Solid State Phys.* **1981**, *14*, L887.
- [16] a) A. Yildiz, N. Serin, T. Serin, M. Kasap, *Jpn. J. Appl. Phys.* **2009**, *48*, 111203; b) A. L. Efros, B. I. Shklovskii, *J. Phys. C: Solid State Phys.* **1975**, *1975*, 49; c) C. O. Yoon, R. M. D. Moses, A. J. Heeger, *Phys. Rev. B* **1994**, *49*, 10851.
- [17] N. F. Mott, E. A. Davis, *Electronic Processes in Non-Crystalline Materials*, Oxford University Press, Oxford **2012**.
- [18] S. Dongmin Kang, G. Jeffrey Snyder, *Nat. Mater.* **2017**, *16*, 252.
- [19] C.-K. Shin, H. Lee, *Synth. Met.* **2004**, *140*, 177.
- [20] a) S. L. Pittelli, D. E. Shen, A. M. Osterholm, J. R. Reynolds, *ACS Appl. Mater. Interfaces* **2018**, *10*, 970; b) Z. Liang, Y. Zhang, M. Souri, X. Luo, A. M. Boehm, R. Li, Y. Zhang, T. Wang, D.-Y. Kim, J. Mei, S. R. Marder, K. R. Graham, *J. Mater. Chem. A* **2018**, *6*, 16495.
- [21] I. H. Jung, C. T. Hong, U. H. Lee, Y. H. Kang, K. S. Jang, S. Y. Cho, *Sci. Rep.* **2017**, *7*, 44704.
- [22] H. Fritzsche, *Solid State Commun.* **1971**, *9*, 1813.
- [23] a) Y. Xuan, X. Liu, S. Desbief, P. Leclère, M. Fahlman, R. Lazzaroni, M. Berggren, J. Cornil, D. Emin, X. Crispin, *Phys. Rev. B* **2010**, *82*, 115454; b) Q. Zhang, Y. Sun, W. Xu, D. Zhu, *Energy Environ. Sci.* **2012**, *5*, 9639; c) S. N. Patel, A. M. Glaudell, K. A. Peterson, E. M. Thomas, K. A. O'Hara, E. Lim, M. L. Chabiny, *Sci. Adv.* **2017**, *3*, e1700434.
- [24] G. H. Kim, L. Shao, K. Zhang, K. P. Pipe, *Nat. Mater.* **2013**, *12*, 719.
- [25] D. Rowe, *Thermoelectrics Handbook*, CRC Press, Boca Raton, FL **2006**.
- [26] a) G. Oustafsson, O. Inoanas, J. O. Nilsson, *Synth. Met.* **1989**, *28*, 427; b) K. Vakiarta, J. Moulton, A. J. Heeger, P. Smith, H. Isotalo, H. Stubb, M. Lojonen, *Synth. Met.* **1991**, *41*, 903; c) Y. Wang, M. F. Rubner, *Synth. Met.* **1990**, *39*, 153; d) M. T. Lojonen, T. Taka, J. Laakso, K. Vikiarta, K. Suuronen, P. Valkeinen, J. E. Österholm, *Synth. Met.* **1991**, *41*, 479.
- [27] D. Emin, *Phys. Today* **1982**, *35*, 34.
- [28] S. K. Yee, N. E. Coates, A. Majumdar, J. J. Urban, R. A. Segalman, *Phys. Chem. Chem. Phys.* **2013**, *15*, 4024.
- [29] S. Ye, M. Steube, E. I. Carrera, D. S. Seferos, *Macromolecules* **2016**, *49*, 1704.